Chaotic Transport and Damping from θ-Ruffled Separatrices

A. A. Kabantsev, Daniel H. E. Dubin, and C. F. Driscoll

Department of Physics, University of California, San Diego, California, USA

Yu. A. Tsidulko

Budker Institute of Nuclear Physics, Novosibirsk, Russia

Variations in magnetic or electrostatic confinement fields give rise to trapping separatrices, and neoclassical transport theory analyzes effects from collision-induced separatrix crossings. Experiments on pure electron plasmas now quantitatively characterize a broad range of transport and wave damping effects due to "chaotic" separatrix crossings, which occur due to equilibrium plasma rotation across θ-ruffled separatrices, and due to wave-induced separatrix fluctuations.

PACS numbers: 52.55.Dy, 52.25.Gj, 52.27.Jt, 52.55.Jd

Most plasma confinement devices have trapping separatrices, arising from variations in magnetic field strength or external potentials. Separately trapped populations of particles may then have substantially different drift orbits, giving rise to large dissipative transport steps when separatrix crossings occur. Neoclassical transport (NCT) theory analyzes the particle transport and wave effects arising from collisional separatrix scatterings in a variety of geometries [1–4], and experimental correspondence has been obtained in some regimes of strong collisions [5,6]. Similarly, recent tokamak experiments have related damping of toroidal rotation to neoclassical viscosity due to weak magnetic ripples [7].

Here we present the first experiments characterizing transport and damping of a novel collisionless form of NCT, where "chaotic" separatrix crossings occur due to plasma rotation across θ-ruffled separatrices, or due to wave-induced separatrix fluctuations. This mechanism has previously been taken to be ineffective because of presumed symmetries [8].

The experiments are performed on low-collisionality, strongly magnetized pure electron plasma columns, with trapping separatrices created by applied wall voltages, or by weak magnetic field strength variations as small as $\delta B/B \sim 10^{-3}$. With near perfect cylindrical symmetry, these plasmas have zero radial expansion, and we apply controlled "error fields," such as a tilt of the magnetic field to induce transport [9]. For wave damping, the error field is the wave potential itself, and strong damping is observed for both low-frequency drift waves and high frequency plasma waves [10].

These experiments with controlled separatrix ruffles and temporal variations now unambiguously distinguish the chaotic and collisional contributions to transport and damping, and distinguish bounce-averaged effects from bounce-resonant effects. For large B, we find that chaotic NCT scales with collision rate and magnetic field as $\nu^0 B^{-1}$, whereas collisional NCT scales as $\nu^{1/2} B^{-1/2}$. The

high magnetic field minimizes kinetic bounce-resonance effects [4,11,12], which typically scale closer to B^{-2}.

Theory analyses of ruffled separatrix effects have now been developed from two complementary perspectives, and will be described separately. A dynamical bounce-mapping approach characterizes the quasi-steady-state density perturbations, including bounce-resonant effects in regimes of ultra-low collisionality. A second simpler approach [13] assumes random (chaotic) separatrix crossings, connects smoothly with collisional NCT, and agrees with the dynamical approach outside the bounce-resonant regimes.

The pure electron plasma columns utilized here are confined in a cylindrical Penning-Malmberg trap [9]. Electrons are confined radially by a nominally uniform axial magnetic field $0.4 < B < 20$ kG; and are confined axially by negative voltages on end cylinders of radius $R_w = 3.5$ cm. The electron columns have length $L_p = 49$ cm, and radial density profile $n(r)$ with central density $n_0 = 1.6 \times 10^7$ cm^{-3} and line density $N_L = \pi R_p^2 n_0 = 6.1 \times 10^7$ cm^{-1}. The unneutralized charge results in an equilibrium potential energy $\Phi_e(r)$ with $\Phi_{e0} = +28$ eV at $r = 0$ (here, all Φ's are in energy units). This gives an $E \times B$ drift-rotation frequency $f_E(r)$ which decreases monotonically from $f_{E0} = 230$ kHz$(B/1 \text{ kG})^{-1}$. The electrons have a near-Maxwellian velocity distribution with thermal energy $T \lesssim 1$ eV, giving axial bounce frequency $f_b = \bar{v}/2L_p = 430$ kHz.

An electrostatic trapping barrier with separatrix energy ϕ_s is created at $z = 0$ by a "squeeze" wall voltage V_{sq} with adjustable θ components. This gives interior separatrix energy $\phi_s(r, \theta) = \phi_{s0}(r) + \Delta\phi_m(r) \cos[m(\theta - \theta_m)]$, as shown schematically in Fig. 1. Here, we consider $m = 2$ ruffles only, created by voltages $\pm\Delta V_m$ applied to four 60° sectors, with $\theta_m = 0.22\pi$. At every radius, low energy particles are trapped in either the left or right end, whereas higher energy untrapped particles transit the entire length. This barrier is similar to the asymmetric magnetic trapping barriers that occur in stellarators and tokamaks.
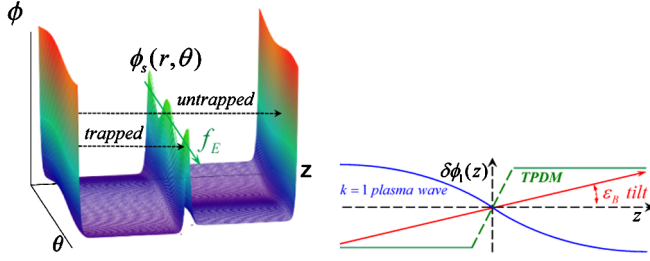
FIG. 1 (color online). Top: θ-symmetric end confinement and central separatrix potentials, modified by an $\ell = 1$ z-antisymmetric error field, and an $m = 2$ ruffle on the separatrix. Bottom: z dependence of three error fields considered here.

FIG. 2 (color online). Measured expansion rate $\nu_{\langle r^2 \rangle}$, showing chaotic NCT varying as $\sin^2(\theta_B - \theta_m)$, and α-independent collisional transport.

Particles change from trapped to untrapped (and vice versa) due to collisions, drift-rotation across θ-ruffles, or temporal fluctuations $\Delta\phi_t$ in the separatrix energy. The electron-electron collisionality of the present experiments is relatively low; collisions acting for a drift-rotation period spread parallel velocities at the separatrix by an energy width $\Delta W_c \equiv T(\nu/2\pi f_E)^{1/2}(\phi_{s0}/T)^{1/2} \approx$ 20 meV$(B/1 \text{ kG})^{1/2}$. The chaotic NCT processes will be important when $\Delta\phi_m \gtrsim \Delta W_c$, or when $\Delta\phi_t \gtrsim \Delta W_c$.

First, we consider radial particle transport. Radial transport is driven by global "error fields" varying as $\delta\phi_\ell \sim e^{i\ell\theta}Z(z)$; here, we consider $\ell = 1$ only, with the three antisymmetric $Z(z)$ dependences shown in Fig. 1. (Notationally, $\delta\phi_\ell$ denotes z-antisymmetric fields which contribute to NCT, and $\Delta\phi_m$ denotes z-symmetric fields which ruffle the separatrix.) For our transport data, the error field is created by a small magnetic tilt with controlled magnitude $\epsilon_B \equiv B_\perp/B_z \lesssim 10^{-3}$ and chosen tilt direction $\theta_B \equiv \tan^{-1}(B_y/B_x)$, i.e., rotated by $\alpha \equiv \theta_B - \theta_m$ relative to the ruffle. This tilt is equivalent to applying wall voltages $V(R_w, \theta, z) = (\epsilon_B z)(2eN_L/R_w) \times \cos(\theta - \theta_B)$, which causes interior Debye-shielded $\ell = 1$ error fields $\delta\phi_1(r, z)$.

Neoclassical transport arises from the difference in drifts in the left and right z-averaged error fields, $\overline{\delta\phi}_L$ and $\overline{\delta\phi}_R$, randomized collisionally and chaotically over separatrix energy widths ΔW_c and $\delta\phi_m$. Theory then gives [13] the radial diffusion coefficient

$$D_r(r) = f_E[(\overline{\delta\phi}_L - \overline{\delta\phi}_R)/\partial_r\Phi_e]^2 \frac{1}{4} F_M(\phi_{s0})$$
$$\times \{\Delta W_c D_{cA} + \Delta\phi_m D_{mA}\sin^2\ell\alpha\},$$
(1)

where F_M is the Maxwellian distribution of energies, the over bar indicates z averaging, and $2\ell/m \in$ Integers. The collisional bounce-averaged coefficient is $D_{cA} \approx \pi\{1 - \exp[-(y/.71)^{5/6}]\}$, $y \equiv \Delta W_c/\Delta\phi_m$, and the m ruffle bounce-averaged coefficient is $D_{mA} \approx 4[1 - .215\tanh(y/.6)]$. These expressions are obtained from the numerical results of Ref. [13] for $m = 2$ and $\ell = 1$.
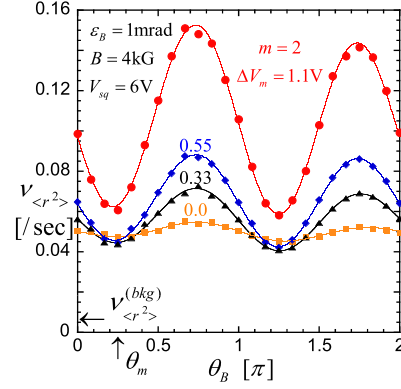
The full radial flux has both mobility and diffusive contributions, as

$$\Gamma_r = -D_r n\partial_r\Phi_e/T - D_r\partial_r n.$$
(2)

Experimentally, we diagnose the bulk expansion rate

$$\nu_{\langle r^2 \rangle} \equiv \frac{d}{dt}\langle r^2 \rangle/\langle r^2 \rangle = \int rdrr^2\frac{1}{r}\partial_r(r\Gamma_r)/\int rdrr^2 n \quad (3)$$

where $\langle r^2 \rangle \equiv \int 2\pi rdrnr^2/N_L$. Fortunately, $\nu_{\langle r^2 \rangle}$ can be accurately and readily obtained from the frequency f_{20} of a diagnostic $m = 2$, $k = 0$ diocotron mode, as $\nu_{\langle r^2 \rangle} = -\frac{d}{dt}f_{20}/f_{20}$. This follows from $f_{20} \propto \langle n \rangle = N_L/2\pi\langle r^2 \rangle$ with N_L constant, and it has been verified to $\pm 2\%$ by camera images of plasma evolutions. The diagnostic mode amplitude is kept small enough so that its effect on transport processes is negligible.

Figure 2 shows measured expansion rate $\nu_{\langle r^2 \rangle}$ versus magnetic tilt direction θ_B, for various applied wall ruffle strengths ΔV_m. The ruffled-induced NCT shows an unambiguous $\sin^2\alpha$ dependence on relative angle α, with magnitude proportional to ΔV_m; and varying θ_m in steps of $\pi/2$ (not shown) verifies the dependence on relative angle only.

The distinctive $\sin^2\alpha$ signature, together with control of V_{sq}, ΔV_m, and ϵ_B, enables experimental identification of bounce-averaged NCT effects separately from bounce-rotation resonance (i.e., kinetic) effects. These transport processes are all quadratic with respect to error field amplitude, so we write

$$\nu_{\langle r^2 \rangle}^{(\text{expt})} = C_{cA}\hat{\epsilon}_B^2 + C_{mA}\hat{\epsilon}_B^2\Delta\hat{V}_m\sin^2\alpha$$
$$+ C_{cK1}\hat{\epsilon}_B^2 + C_{cK2}\Delta\hat{V}_m^2 + \nu_{\langle r^2 \rangle}^{(\text{bkg})}. \quad (4)$$

Here, C_{cA} and C_{mA} represent radial integrals of the bounce-averaged Eqs. (1)–(3). This separatrix-dependent NCT is called "superbanana" in toroidal systems; and with the presumption of $\alpha = 0$, a ν' regime of (weaker) transport replaces our $\nu^{1/2}$ regime [8]. The C_{cK1} and C_{cK2} coefficients represent "standard" plateau-regime NCT,
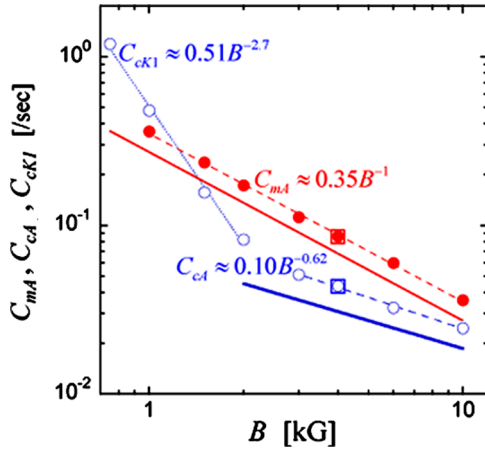
FIG. 3 (color online). Measured transport rates C versus magnetic field B, with empirical scalings. Solid lines are theory predictions.

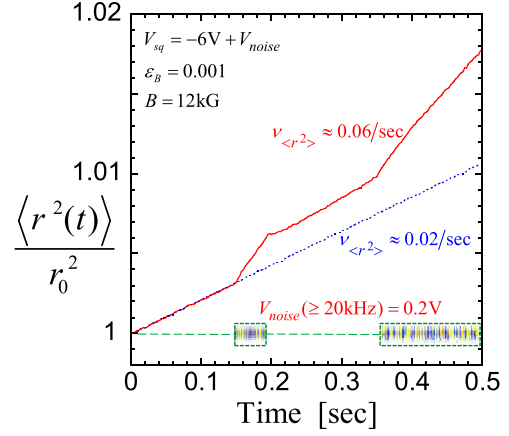

FIG. 4 (color online). Enhanced expansion rate during two bursts of 200 mV (rms) noise applied to a 6 V electrostatic separatrix.

with collisions randomizing bounce-resonant orbits steps [1,4] driven by the tilt and ruffle error fields. This separatrix-independent NCT is called "axi-symmetric" in toroidal systems [8]. The residual $\nu_{\langle r^2 \rangle}^{(bkg)}$ represents transport from uncontrolled background error fields, separatrices, and ruffles. For dimensional simplicity, $\hat{\epsilon}_B = \epsilon_B(1 \text{ m Rad})$ and $\Delta \hat{V}_m \equiv \Delta V_m/(1 \text{ Volt})$.

Experimentally, C_{mA} is readily obtained from the $\sin^2 \alpha$ dependence as in Fig. 2, and varying ϵ_B gives the expected ϵ_B^2 dependence. Data taken with $\epsilon_B = 0$ show a $\nu_{\langle r^2 \rangle}^{(bkg)}$ offset and a parabolic dependence on applied ΔV_m, giving C_{cK2}. Varying ϵ_B then selects C_{cA} and C_{cK1}; these are distinguished only by their B scaling (discussed next), and by the fact that the bounce-averaged differences in C_{cA} require the separatrix, whereas the kinetic C_{cK1} depends only weakly on the applied squeeze voltage.

Figure 3 shows the measured transport rates C_{mA}, C_{cA}, and C_{cK1} versus magnetic field with empirical scalings (dashed), compared to theory Eqs. (1)–(3) (lines). At high B, the chaotic and collisional neoclassical coefficients C_{mA} and C_{cA} agree closely with theory, scaling as B^{-1} and $B^{-1/2}$ respectively. Here the comparison is limited by temperature uncertainty, sensitivity to edge density gradients, and induced modification of $F_M(\phi_{s0})$. At low B, the kinetic transport labeled C_{cK1} is observed to depend strongly on field ($\sim B^{-2.7}$), but no simple power law is expected as bounce-rotation resonances become dominant. Prior transport scaling experiments have been confused by the presence of uncontrolled separatrices and ruffles, and by overlapping transport regimes [9].

Similar enhanced transport is observed when there are temporal variations $\Delta \phi_t$ in the separatrix energy. Figure 4 illustrates the immediate increase in radial expansion rate induced when white noise ($V_{RMS} = 200$ mV, $f_{E0} < f < 20$ MHz) is applied to the θ-symmetric squeeze ring, causing chaotic trapped-passing transitions. The $3\times$ increase in

$(d/dt)\langle r^2 \rangle$ observed here is consistent with a collisional separatrix layer $\Delta W_c \sim 70$ meV fluctuating by $\Delta \phi_t \sim 200$ meV. Presumably, any noise or wave-induced fluctuations which change particle kinetic energies relative to the separatrix energy would be equally effective in enhancing transport.

Next, we consider wave damping due to chaotic and collisional separatrix dissipation. Damping has now been observed for both negative-energy $E \times B$ drift waves and for positive-energy plasma waves. Here, the wave-potential is the "error field" driving transport [Fig. 1], and the wave frequency enters the generalization of Eq. (1). Most thoroughly studied is the $\ell = 1$ "Trapped Particle Diocotron Mode" (TPDM) [3] where end-trapped particles at large radii experience z-antisymmetric $E \times B$ drifts, while untrapped interior particles provide partial Debye shielding.

Prior TPDM damping analysis [3] solved for the thin collisional boundary layer at the separatrix, as is standard in NCT [1,2]. This gave quantitative agreement with the experimental observations of $\gamma_{1a} \propto B^{-1/2}$ for large B, but the enhanced damping observed at lower B, scaling as $\gamma_{1a} \propto B^{-1}$, was not understood.

Experiments and theory now quantify the B^{-1} scaling of TPDM damping as due to θ ruffles on the separatrix. Figure 5(a) shows the measured TPDM damping rate γ_{1a} versus strength ΔV_m of an applied $m = 2$ separatrix ruffle for two magnetic fields. For $\Delta V_m = 0$, the damping is mostly due to collisions; for larger ΔV_m, the damping increases linearly with ΔV_m as expected for chaotic NCT. Here, $\gamma_{1a} * B$ is plotted, so the identical slopes at $B = 0.4$ and $B = 3$ represent the B^{-1} scaling characteristic of chaotic separatrix processes, analogous to the ΔV_m terms of Eq. (1). In contrast, the collisional $\Delta V_m = 0$ intercepts scale as $B^{-1/2}$, and therefore differ by $(3/0.4)^{1/2} = 2.7$. The solid curves of Fig. 5(a) are the
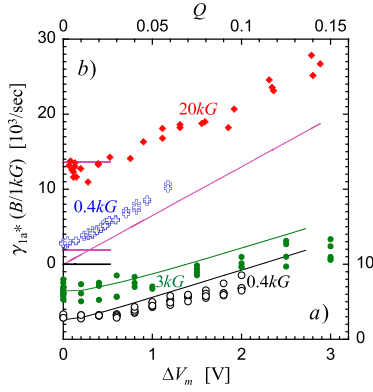
FIG. 5 (color online). (a) (bottom, right scales) TPDM damping rate γ_{1a} times B versus applied $m = 2$ ruffle ΔV_m for $B = 0.4$ and 3.0 kG. (b) (top, left scales) damping versus amplitude Q of an excited $m = 2$ diocotron mode.

absolute predictions of the probabilistic theory approach, including collective effects [14] on $n(r, z)$ equilibria.

Similar enhanced damping is seen when a separate wave ruffles the separatrix. Figure 5(b) shows TPDM damping in the presence of a separate $m = 2$, $k = 0$ diocotron mode with frequency $f_{20} \approx f_{E0}$ and controlled quadrupole amplitude Q. Here Q would be Δ/R_0 for uniform density out to radius $R = R_0 + \Delta \cos 2\theta$. The diocotron mode creates an $m = 2$ potential $\phi_2(r, z, t)$ at all z, which is smallest at the $z = 0$ separatrix, inducing chaotic separatrix crossings proportional to Q. The solid line segments show a $Q = 0$ intercept predicted by collisional NCT [3], and a ruffle-induced enhancement predicted by the bounce-mapping theory, in good agreement with the measurements.

High frequency plasma waves are also strongly damped by separatrix dissipation, independent of Landau damping effects, but critically dependent on the characteristics of the separatrix [10]. Figure 6 shows the measured damping rate γ_{11} for an $\ell = 1$, $k = 1\pi/L_p$ plasma wave with

$f_{11} = 1.2$ MHz. This is a large amplitude wave in a "BGK state" of strong wave-particle trapping. With no applied electrostatic squeeze, damping at rate $\gamma_{11}^{(M)} \sim -1 \times 10^3/$ sec is observed, due to a naturally occurring magnetic separatrix $\delta B/B \sim 10^{-3}$ peaking near $z = 0$. This magnetic separatrix often dominates background transport also, and removing the separatrix reduces $\nu_{\langle r^2 \rangle}^{(bkg)}$ by up to $5 \times$.

In Fig. 6, adding a ramped positive θ-symmetric wall voltage V_{sq} has no effect on γ_{11} since it creates no barrier, but a negative squeeze ramped to -3 Volts immediately and proportionately increases γ_{11}, to a maximum of $\gamma_{11}^{(3V)} = -8 \times 10^3/$ sec. Here, Zakharov-Karpman [15] collisional damping predicts negligible damping, at a rate $\gamma_{11}^{ZK} \sim -20/$ sec. We also note that when a separatrix is present, excitation of a separate $m = 0$ plasma wave to even moderate amplitude immediately increases γ_{11} several fold, due to fluctuations $\Delta \phi_t$ in the effective energy of the separatrix. However, quantitative understanding of separatrix damping of wave-induced currents is not yet complete.
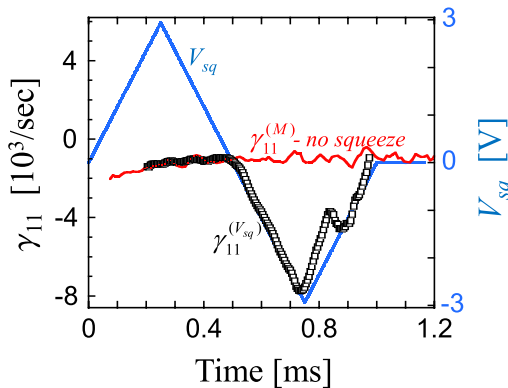
FIG. 6 (color online). Separatrix damping of a Langmuir wave: $\gamma_{11}^{(M)}$ from a weak magnetic mirror (red), and $\gamma_{11}^{(V_{sq})}$ (black) due to a ramped θ-symmetric negative V_{sq} (blue).

[1] F. L. Hinton and R. D. Hazeltine, Rev. Mod. Phys. **48**, 239 (1976).
[2] M. N. Rosenbluth, D. W. Ross, and D. P. Kostamorov, Nucl. Fusion **12**, 3 (1972).
[3] T. J. Hilsabeck and T. M. O'Neil, Phys. Plasmas **10**, 3492 (2003).
[4] D. H. E. Dubin, Phys. Plasmas **15**, 072112 (2008).
[5] T. Ohkawa, J. R. Gilleland, and T. Tamano, Phys. Rev. Lett. **28**, 1107 (1972).
[6] M. C. Zarnstorff, K. McGuire, M. G. Bell, B. Grek, D. Johnson, D. McCune, H. Park, A. Ramsey, and G. Taylor, Phys. Fluids B **2**, 1852 (1990).
[7] M. F. F. Nave *et al.*, Phys. Rev. Lett. **105**, 105005 (2010).
[8] H. E. Mynick, Phys. Plasmas **13**, 058102 (2006); H. E. Mynick, Phys. Fluids **26**, 2609 (1983).
[9] A. A. Kabantsev and C. F. Driscoll, Phys. Rev. Lett. **89**, 245001 (2002).
[10] A. A. Kabantsev and C. F. Driscoll, Phys. Rev. Lett. **97**, 095001 (2006).
[11] D. L. Eggleston and T. M. O'Neil, Phys. Plasmas **6**, 2699 (1999); D. L. Eggleston and J. M. Williams, Phys. Plasmas **15**, 032305 (2008).
[12] E. P. Gilson and J. Fajans, Phys. Rev. Lett. **90**, 015001 (2003).
[13] D. H. E. Dubin, C. F. Driscoll, and Yu. A. Tsidulko, Phys. Rev. Lett. **105**, 18503 (2010).
[14] T. Akhmetov and I. Kotelnikov, Phys. Plasmas **16**, 122103 (2009).
[15] V. E. Zakharov and V. I. Karpman, Sov. Phys. JETP **16**, 351 (1963).